JBC RESEARCH ARTICLE

Deciphering functional redundancy and energetics of malate oxidation in mycobacteria

Received for publication, August 5, 2021, and in revised form, March 20, 2022 Published, Papers in Press, March 23, 2022,
https://doi.org/10.1016/j.jbc.2022.101859

Liam K. Harold[1,2,*], Adrian Jinich[3], Kiel Hards[1,2], Alexandra Cordeiro[3], Laura M. Keighley[1], Alec Cross[1], Matthew B. McNeil[1,2], Kyu Rhee[3], and Gregory M. Cook[1,2,*]

From the [1]Department of Microbiology and Immunology, School of Biomedical Sciences, University of Otago, Dunedin, New Zealand; [2]Maurice Wilkins Centre for Molecular Biodiscovery, The University of Auckland, Auckland, New Zealand; [3]Division of Infectious Diseases, Weill Department of Medicine, Weill Cornell Medical College, New York, New York, USA

Edited by Chris Whitfield

Oxidation of malate to oxaloacetate, catalyzed by either malate dehydrogenase (Mdh) or malate quinone oxidoreductase (Mqo), is a critical step of the tricarboxylic acid cycle. Both Mqo and Mdh are found in most bacterial genomes, but the level of functional redundancy between these enzymes remains unclear. A bioinformatic survey revealed that Mqo was not as widespread as Mdh in bacteria but that it was highly conserved in mycobacteria. We therefore used mycobacteria as a model genera to study the functional role(s) of Mqo and its redundancy with Mdh. We deleted *mqo* from the environmental saprophyte *Mycobacterium smegmatis*, which lacks Mdh, and found that Mqo was essential for growth on nonfermentable carbon sources. On fermentable carbon sources, the *Δmqo* mutant exhibited delayed growth and lowered oxygen consumption and secreted malate and fumarate as terminal end products. Furthermore, heterologous expression of Mdh from the pathogenic species *Mycobacterium tuberculosis* shortened the delayed growth on fermentable carbon sources and restored growth on nonfermentable carbon sources at a reduced growth rate. In *M. tuberculosis*, CRISPR interference of either *mdh* or *mqo* expression resulted in a slower growth rate compared to controls, which was further inhibited when both genes were knocked down simultaneously. These data reveal that exergonic Mqo activity powers mycobacterial growth under nonenergy limiting conditions and that endergonic Mdh activity complements Mqo activity, but at an energetic cost for mycobacterial growth. We propose Mdh is maintained in slow-growing mycobacterial pathogens for use under conditions such as hypoxia that require reductive tricarboxylic acid cycle activity.

Bacteria frequently encode multiple enzymes for the same metabolic reactions, but it is not understood whether such enzymes are functionally redundant or possess differential roles. A critical step in central metabolism is the oxidation of malate, which can be performed by either malate dehydrogenase (Mdh) or malate quinone oxidoreductase (Mqo). Bacteria can encode varying combinations of these enzymes, but the physiological consequences behind each permutation are not well understood. In this communication, we compared the role of malate oxidation in the fast-growing soil actinomycete *Mycobacterium smegmatis*, which encodes only Mqo, and the closely related slow-growing human pathogen *Mycobacterium tuberculosis*, which encodes both Mqo and Mdh. We show that energization of the electron transport chain by exergonic Mqo is critical for powering aerobic mycobacterial growth and that there is an energetic cost to using endergonic Mdh under these conditions. Mdh has been conserved by mycobacterial species that require growth and survival under diverse physiological states.

The tricarboxylic acid (TCA) cycle, which links energy generation to carbon flux, is central to the carbon metabolism of many organisms in the communities responsible for essential life processes. In aerobic organisms, the TCA cycle is used to release stored chemical energy from acetyl-CoA (1). Malate oxidation is a critical step for the completion of the TCA cycle and the regeneration of oxaloacetate. Two predominant enzymes have evolved that are capable of malate oxidation to oxaloacetate, malate dehydrogenase (Mdh) and malate quinone oxidoreductase (Mqo). Studies on malate oxidation have primarily focused on Mdh, while Mqo investigation has been limited. There is an alternative path for malate oxidation out of the TCA cycle using malic enzyme (Mez), a member of the anaphoretic node. Mez performs the oxidative decarboxylation of malate to pyruvate producing NAD(P)H from NADP (2).

Mqo is a monotopic membrane protein that utilizes a FAD cofactor to couple malate oxidation to quinone reduction, thereby providing a link between central carbon metabolism and the electron transport chain (3–6). Coupling malate oxidation to quinone reduction is exergonic (thermodynamically favorable) giving Mqo an energetic advantage over Mdh. Malate oxidation using Mdh is highly endergonic (unfavorable) when coupled to the reduction of NAD^+ with an apparent standard Gibbs reaction energy of +30 kJ/mol at pH = 7 (5–7). Due to this thermodynamic unfavorability, Mdh has evolved mechanisms, in combination with other energetically favorable enzymes, such as crosstalk and substrate channeling to enable malate oxidation (8, 9). Mqo and Mdh

* For correspondence: Liam K. Harold, liamharold@gmail.com; Gregory M. Cook, greg.cook@otago.ac.nz.

commonly co-occur within a single bacterium, with one enzyme being primarily responsible for malate oxidation (4, 5). In *Escherichia coli*, Mdh is responsible for malate oxidation under aerobic conditions with Mqo having no prescribed role (4). Conversely, in *Corynebacterium glutamicum*, Mqo is the primary driver of malate oxidation with Mdh proposed to operate in the reductive direction (5). Mez is also present in *E. coli* and does not take over the role of Mqo during growth (4). Some bacteria such as *Mycobacterium smegmatis*, an environmental saprophyte, have lost the Mdh enzyme from their genome altogether, and no Mdh activity is detected in this bacterium (10, 11). Human pathogens from the same genus have lost Mqo (*e.g.*, *Mycobacterium leprae*) or maintained both enzymes (*e.g.*, *Mycobacterium tuberculosis*) (10, 11). It is not currently understood why loss of either enzyme occurs or what drives conservation of both enzymes for malate oxidation in different mycobacterial species.

In mycobacteria, some species such as *M. tuberculosis* utilize Mdh to facilitate a reductive TCA cycle to produce fumarate for use as a terminal electron acceptor (12). This provides an alternative electron acceptor for *M. tuberculosis* in conditions of hypoxia thereby providing a mechanism to maintain the membrane potential and recycle reducing agents. In contrast, *M. smegmatis* does not have the ability to catalyze either of these reactions but has evolved alternative mechanisms to recycle reducing equivalents such as hydrogenases (13–15). In *C. glutamicum*, a close relative of Mycobacteria, both functionally active Mqo and Mdh enzymes are present and catalyze cyclic conversions of malate and oxaloacetate (5). Mqo is the most physiologically important enzyme in *C. glutamicum* for malate oxidation, and Mdh plays a role in oxaloacetate reduction (5). The net reaction of Mqo and Mdh is equivalent to NADH:quinone oxidoreductase (type II–NDH-2) and may play a role as an additional NDH-2 or be involved in the regulation of malate or oxaloacetate concentrations (5). *M. tuberculosis* can also use Mqo and Mdh in combination to form a futile cycle to provide a pseudo NDH-2–type enzyme (16).

Currently, there is a mismatch between the energetic favorability of Mqo and what is observed in nature with greater use of the Mdh enzyme for malate oxidation. Therefore, we undertook a study to investigate the role of Mqo and Mdh in mycobacterial physiology. We performed a bioinformatic, molecular, and energetic analysis of the proteins from *M. smegmatis* (Mqo *MSMEG_2613*) and *M. tuberculosis* (Mqo *Rv2852c* and Mdh *Rv1240*) to assess functional redundancy and the physiological role of Mqo and Mdh.

Results and discussion

Prevalence of Mqo and Mdh enzyme in bacteria

To gain a more extensive insight into the roles and redundancy of Mqo (Fig. 1*A*) and Mdh (Fig. 1*B*) in bacteria, we performed an analysis of 6250 unique bacterial proteomes to understand the prevalence and distribution of the enzymes (Fig. 1). This analysis revealed that Mdh is the dominant mechanism for converting malate to oxaloacetate being found in 69% of bacterial species compared to 27% of species possessing Mqo. Interestingly, 19% of bacterial species possess both enzymes, and 23% of species possess neither enzyme (Fig. 1*C*). Eight percent of species possessed an orphaned Mqo with the highest occurrence in the Nocardiaceae, Geodermatophilaceae, Microbacteriaceae, Micrococcaceae, Sphingobacteriales, Synechococcaceae, Campylobacterales, Oceanospirillales, Pseudomonadales, and Thiotrichales families and orders (Fig. 1*C*).

Mqo was enriched for in the Mycobacteriaceae, with 94 of 100 species in possession of a *mqo* operon (Fig. 1*D*). Several mycobacterial species (13 out of 100), including *M. smegmatis* and the entire *Mycobacterium abscessus* complex, contained only Mqo (Fig. 1*D*). Notably, all of the species with a single Mqo are fast growing mycobacteria. In contrast, slow growing pathogenic mycobacteria harbored both Mqo and Mdh enzymes with the exception of *M. leprae* with a single Mdh, a bacterium that has undergone significant reductive evolution and cannot be cultured *in vitro* (Fig. 1*D*). The Mycobacteriaceae that maintain both Mqo and Mdh may use a reductive TCA cycle in hypoxic conditions they encounter thereby driving conservation of these enzymes for both optimal growth during energy rich periods (Mqo) and survival and maintenance during hypoxia (Mdh). The high conservation of Mqo at the expense of Mdh in the Mycobacteriaceae family suggests that Mqo plays a critical role in carbon and energy metabolism for these organisms.

The *mqo* gene of M. smegmatis encodes for a functional Mqo enzyme that is obligatory for growth on nonfermentable carbon sources

To gain molecular insight into the role of Mqo in mycobacterial species, we created a gene deletion of *mqo* in *M. smegmatis* and CRISPRi knockdown strains of *mqo* and *mdh* in *M. tuberculosis*. The *M. smegmatis* Δ*mqo* deletion mutant was constructed using a hygromycin resistance marker and confirmed using whole genome sequencing and various assays to measure Mqo enzyme activity (Fig. 2).

The respiratory chain activity of Mqo in *M. smegmatis* was validated biochemically using inverted membrane vesicles (IMVs). When IMVs were energized with malate as the sole electron donor (ΔG° = −19 kJ/mol), malate-dependent proton-pumping (quenching of 9-amino-6-chloro-2-methoxyacridine [ACMA]) was observed demonstrating that Mqo was membrane-bound and part of the electron transport chain in *M. smegmatis* (Fig. 2*A*). A similar trend is observed by feeding electrons into the respiratory chain at complex II (succinate dehydrogenase) using succinate, but the level of proton pumping activity was lower possibly reflecting the endergonic nature of this reaction (ΔG° = +21 kJ/mol) in mycobacteria (17). For both malate and succinate, ACMA quenching was reversed by the protonophore carbonyl cyanide *m*-chlorophenyl hydrazine (CCCP) validating the formation of a protonmotive force in these IMVs (Fig. 2*A*). These data demonstrated that in *M. smegmatis* Mqo was a membrane-bound protein that oxidized malate coupled to the reduction of quinones in the electron transport chain.

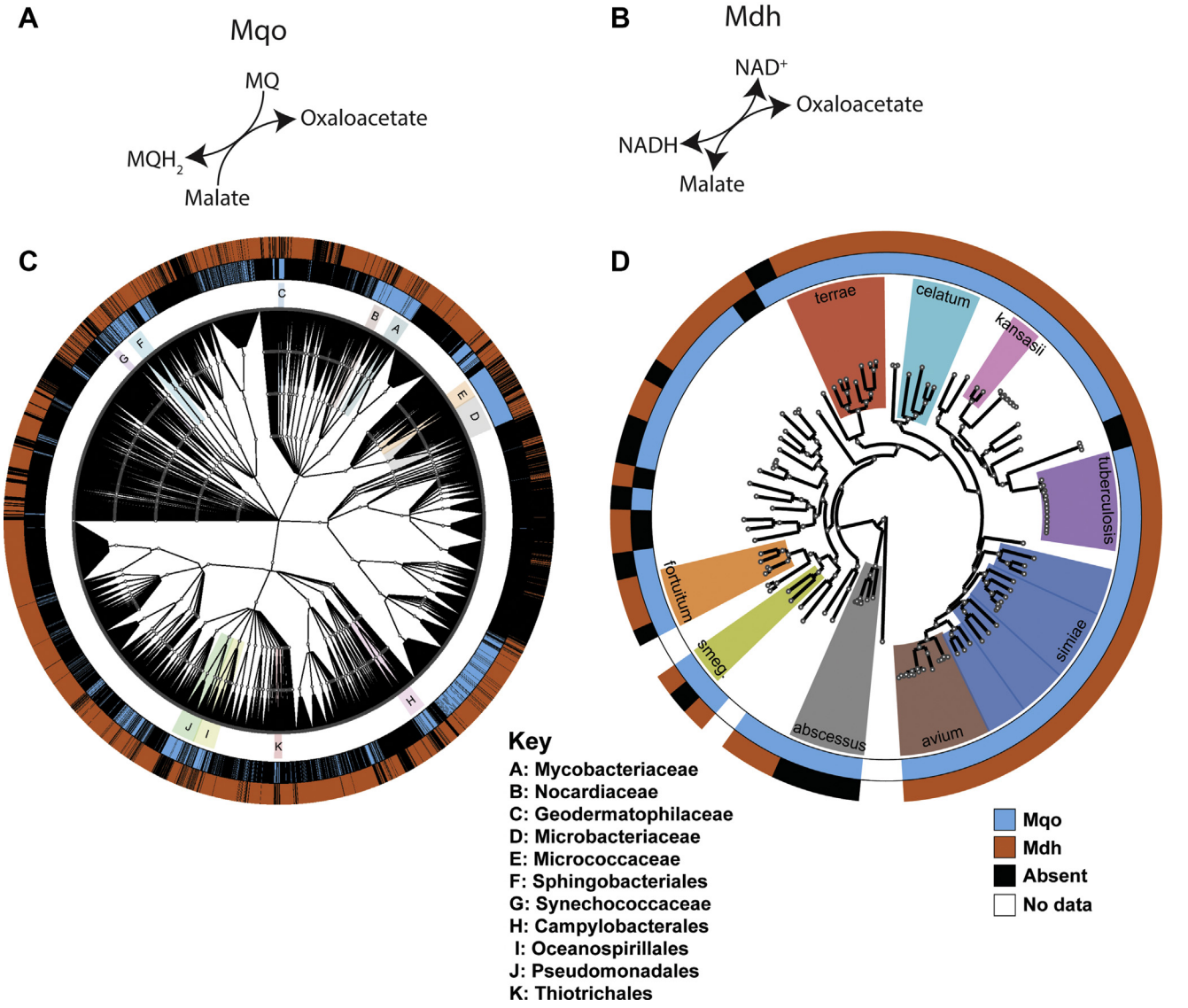

Figure 1. Prevalence of malate dehydrogenase (Mdh) and malate quinone oxidoreductase (Mqo) enzymes in bacteria and Mycobacteria. *A*, Mqo and *B*, Mdh enzyme reactions. *C*, visualization of combination of Mqo and Mdh present in each UniProt *reference* bacterial proteomes with the absence (*black*) or presence of Mqo (*blue*) and Mdh (*orange*) indicated in surrounding colored coded rings created using GraPhlAn. Families and orders highlighted represent the top ten families/orders with the highest fraction of species with orphaned Mqo, except Mycobacteriaceae (minimum 20 species). *D*, phylogeny of mycobacteria taken from Fedrizzi *et al.* (42) and reconstructed using GraPhlAn to show the presence or absence of Mqo and Mdh indicated in surrounding colored coded rings. *Colored clades* represent different mycobacterial complexes.

To study oxygen consumption in IMVs and to determine the impact of Mqo on respiration, we measured both NADH-dependent and malate-dependent oxygen consumption rates (OCRs) in the WT and Δ*mqo* deletion mutant (Fig. 2*B*). High rates of oxygen consumption were detected in the WT with both electron donors. NADH-dependent oxygen consumption was lower in the Δ*mqo* mutant compared to the WT, and malate-dependent oxygen consumption was near the limit of detection validating the deletion of *mqo* in the mutant (Fig. 2*B*). We studied the Δ*mqo* mutant further by measuring the enzyme activity of Mqo directly by measuring malate oxidation in IMVs coupled to phenazine ethosulfate–2,6 dichlorophenolindophenol (DCIP) (Fig. 2*C*). The rate of malate oxidation in the WT was 83 ± 0.6 nmol malate min^{-1} mg^{-1} protein, and this was reduced to 0.3 ± 0.03 nmol malate min^{-1} mg^{-1} protein in the Δ*mqo* deletion mutant (Fig. 2*C*). These results confirmed there was no compensatory mechanism of malate oxidation in the electron transport chain of *M. smegmatis* Δ*mqo*, and Mqo deletion had a negative effect on the other respiratory chain components operating effectively.

At a physiological level, the Δ*mqo* mutant had significantly altered growth kinetics compared to the isogenic WT on fermentable carbon sources, and no growth was observed on nonfermentable carbon sources (Fig. 3). Growth of the Δ*mqo* mutant on either glycerol or glucose as the sole carbon and energy source was always delayed with a lower final A_{600} relative to the WT (Fig. 3*A*). To determine if the growth of the Δ*mqo* mutant after the long lag phase was the result of a suppressor mutation on these carbon sources, we plated the grown culture on solid media and regrew the resulting colonies on the fermentable carbon source glycerol. We then analyzed the growth kinetics of these individual colonies and

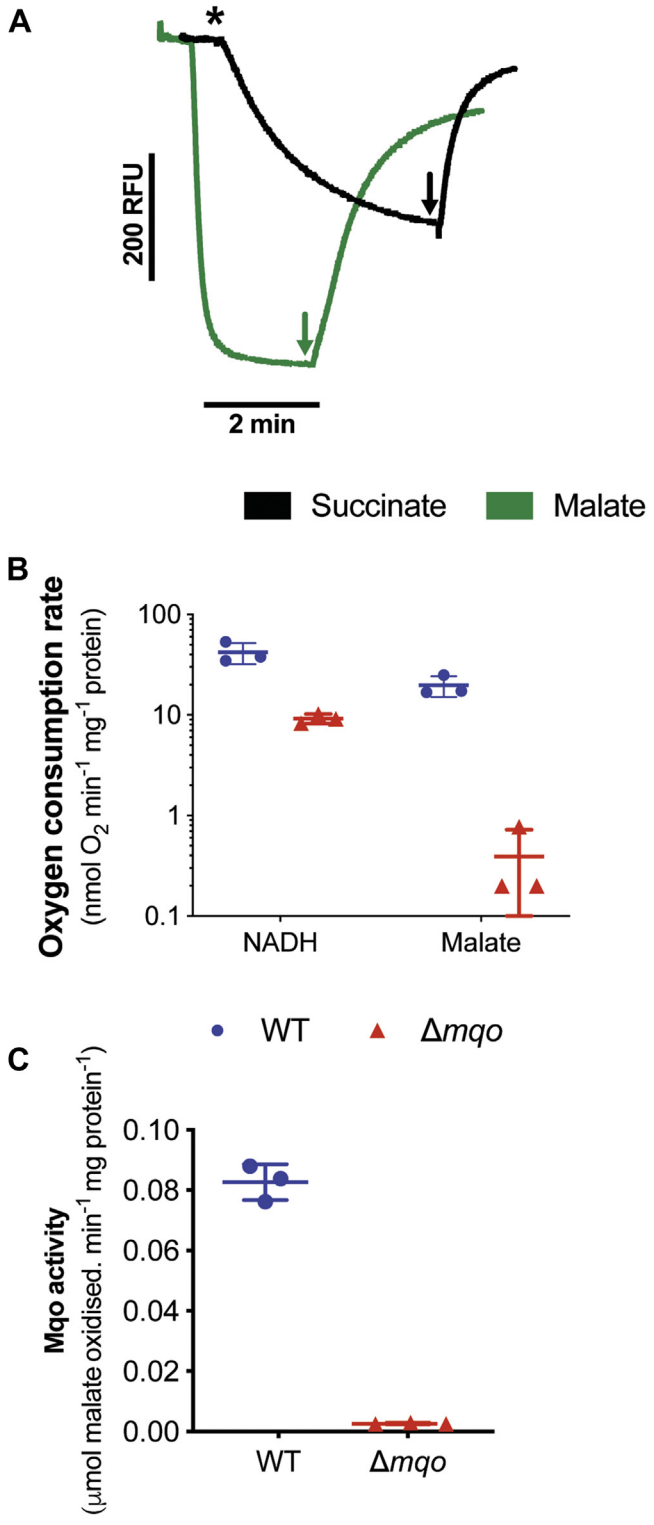

Figure 2. Activity of Mqo in IMVs of *M. smegmatis*. *A*, succinate- and malate-driven proton translocation in IMVs of *M. smegmatis*. Quenching of ACMA fluorescence in IMVs was initiated with either 5 mM succinate or 5 mM malate (* final concentration), and at the indicated time points (*arrows*), the uncoupler carbonyl cyanide *m*-chlorophenyl hydrazine (CCCP) at 50 μM was added to collapse the proton gradient (reversal of ACMA fluorescence). Experiments are representative of a technical triplicate. *B*, oxygen consumption rates of IMVs prepared from the WT (*closed blue circles*) and the Δ*mqo* mutant (*closed red triangles*) with either NADH or malate as an electron donor (5 mM each). *C*, activity of Mqo in IMVs prepared from the WT (*closed blue circles*) and the Δ*mqo* mutant (*closed red triangles*). Data in (*B*) and (*C*) are an average of biological triplicates with error bars representing standard deviation. ACMA, 9-amino-6-chloro-2-methoxyacridine; IMVs, inverted membrane vesicles; Mqo, malate quinone oxidoreductase.

found that the regrown colonies still maintained the growth defect observed in the original Δ*mqo* mutant indicating they were not suppressor mutants and that growth of the Δ*mqo* mutant was a physiological adaption (Fig. 3*B*).

One possible mechanism for *M. smegmatis* to reroute malate in the TCA cycle in the absence of Mqo is to use Mez to catalyze the reversible decarboxylation of malate to pyruvate with concomitant reduction of $NAD(P)^+$. In *M. tuberculosis*, Mez (Rv2332) is not required for growth on gluconeogenic or glycolytic substrates, and the major role proposed for this enzyme in *M. tuberculosis* is as a L-malate decarboxylase to produce NAD(P)H for lipid biosynthesis (18). To confirm that Mez activity was not responsible for the growth of the *M. smegmatis* Δ*mqo* mutant, we measured the activity of Mez in the cytosolic fraction of the Δ*mqo* mutant created during the preparation of IMVs and compared it to the WT (Fig. 3*C*). We found that the Δ*mqo* mutant had lower activity of Mez relative to the WT, indicating it was probably not compensating for the deletion of Mqo (Fig. 3*C*). When grown with strictly nonfermentable carbon sources like succinate, malate, or acetate, the Δ*mqo* mutant was unable to grow even after 200 h of incubation demonstrating the essential requirement for a functional Mqo enzyme under these conditions (Fig. 3*D*).

To determine if this lack of growth on nonfermentable carbon sources was due to the inability of cells to oxidize these carbon sources, cells were grown on glycerol and their respiratory capacity measured with various electron donors (Fig. 3*E*). When either glycerol or succinate was used as an electron donor for respiration, the WT respired at a rate of 126 nmol O_2 min^{-1} mg^{-1} protein and 72 nmol O_2 min^{-1} mg^{-1} protein, respectively (Fig. 3*E*). In contrast, the OCR of the Δ*mqo* mutant was 69 nmol O_2 min^{-1} mg^{-1} protein and 8.26 nmol O_2 min^{-1} mg^{-1} protein on glycerol and succinate, respectively (Fig. 3*E*). We concluded from these experiments that the Δ*mqo* mutant had significantly reduced capacity to oxidize nonfermentable carbon sources to power growth. To further evaluate these differences in OCR, we tested the maximum respiratory capacity of the cells by using the protonophore CCCP to fully uncouple the electron transport chain leading to stimulation of the OCR (19, 20). We define the spare respiratory capacity of the cell as the difference between the OCR (minus CCCP) and the maximal CCCP-activated OCR. With either glycerol or succinate as the electron donor, the WT cells showed high rates of stimulation by CCCP, *i.e.*, spare respiratory capacity (Fig. 3*E*). The Δ*mqo* mutant had very little spare respiratory capacity as assessed by the lack of CCCP activation of OCR (Fig. 3*E*). Overall, these data show that the Δ*mqo* mutant had a lower OCR with electron donors that feed directly into the electron transport chain.

The Δmqo mutant secretes malate and undergoes succination of metabolites

During growth on glycerol, we observed that the Δ*mqo* mutant acidified the growth medium to a final pH value of

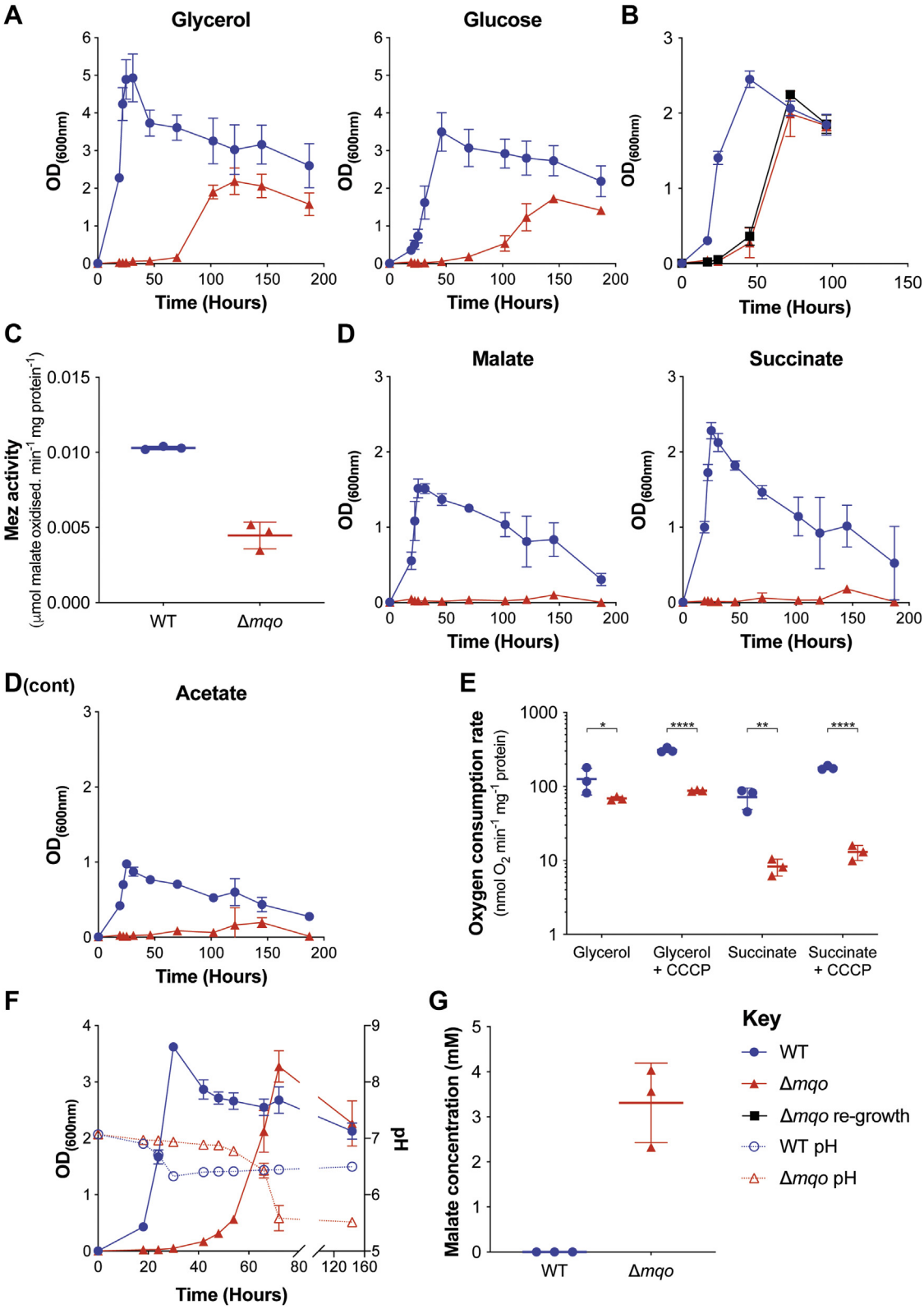

Figure 3. *M. smegmatis* Δ*mqo* mutant has delayed growth on fermentable carbon sources and is unable to grow on nonfermentable carbon sources. *A*, growth of the Δ*mqo* mutant (*solid red triangles*) compared to WT (*solid blue circles*) on HdB minimal medium with the fermentable carbon sources glycerol (22 mM) or glucose (20 mM). *B*, regrowth of Δ*mqo* mutant on HdB minimal medium with glycerol (22 mM) following adaptation on glycerol (*solid black squares*). *C*, malic enzyme (Mez) activity of cytoplasmic fractions prepared from the Δ*mqo* mutant compared to WT. *D*, growth of the Δ*mqo* mutant (*solid red triangles*) compared to WT (*solid blue circles*) on HdB minimal medium with the nonfermentable carbon sources malate (20 mM), succinate (20 mM), or acetate (20 mM). *E*, oxygen consumption rates of washed cell suspensions energized with either glycerol (5 mM) or succinate (5 mM). CCCP was added at 10 μM (final concentration): Δ*mqo* mutant (*solid red triangles*), WT (*solid blue circles*). Two-way ANOVA with Sidaks multiple comparisons: *$p < 0.05$, **$p < 0.01$, ****$p < 0.0001$. *F*, growth (solid blue circle and solid red triangle) and external pH (open *symbols*) of the Δ*mqo* mutant (*red triangles*) compared

5.52 ± 0.08, in comparison to pH 6.33 ± 0.02 for the WT (Fig. 3*F*). This indicated that the Δ*mqo* mutant was secreting an acidic end product into the growth medium. We initially hypothesized that the Δ*mqo* mutant secretes one or several dicarboxylic acid intermediates of the TCA cycle as the acidic end product causing the lower pH of the medium. To test this hypothesis, we performed comparative targeted metabolomics of intracellular and secreted metabolites for the Δ*mqo* mutant and the WT. While extracellular malate was undetectable in the WT, we detected high levels of secreted malate in the growth medium of the Δ*mqo* mutant (Fig. 3*G*). To quantify the level of malate secreted into HdB liquid medium, we used a colorimetric enzymatic assay and found an average concentration of 3.3 ± 0.88 mM for the Δ*mqo* mutant, compared to no detectable levels for WT (Fig. 3*G*). Notably, this malate excretion represents about 20% of the total carbon supplied in the growth medium. Furthermore, extracellular levels for both fumarate and succinate, the two metabolites upstream of malate in the TCA cycle, had an average log2-fold increase of 8 and 2 in the Δ*mqo* mutant relative to WT, respectively (Fig. 4).

To determine what was causing the secretion of these metabolites, we examined the levels of intracellular TCA metabolites. We found the intracellular TCA cycle metabolites were significantly altered with intracellular levels of malate, fumarate, succinate, and citrate having an average log2-fold increases relative to WT of 12, 8, 4, and 3, respectively (Fig. 4). Interestingly, the abundance of alpha-ketoglutarate decreased relative to WT by an average log2-fold change of −2, and the average abundance of glutamate was unchanged (Fig. 4). Thus, disrupting *mqo* results in significant build-up of TCA cycle intermediates upstream of the malate oxidation reaction, with concomitant secretion of malate, fumarate, and succinate. The lack of alpha-ketoglutarate build-up suggests that a large portion of carbon flows from isocitrate to malate and succinate through the glyoxylate shunt, bypassing isocitrate dehydrogenase and alpha-ketoglutarate dehydrogenase. However, except in the case of malate synthase mutants (21), the levels of the one intermediate of the glyoxylate shunt (*i.e.*, glyoxylate) exhibits very little variation and therefore it is challenging to use experimentally as a proxy for changes in metabolic flux through the glyoxylate bypass. This tight regulation of glyoxylate levels is likely an evolutionary mechanism to manage the documented toxicity of the aldehyde functional group of excess glyoxylate (21) and is mechanistically likely due to the higher catalytic efficiency of malate synthase in comparison to isocitrate lyase.

These metabolomic data demonstrate that deletion of *mqo* in *M. smegmatis* causes a back-up in the TCA cycle forcing the cell to excrete several dicarboxylic acid intermediates of the TCA cycle to achieve growth on fermentable carbon sources. However, the excretion of TCA intermediates does not provide a strategy to rescue growth on nonfermentable carbon sources. The drop in the pH of the growth medium due to the excretion of these intermediates may provide a potential mechanism to cause down regulation of components of the electron transport chain manifested as lowered oxygen consumption (see Fig. 3*E*). Mechanistically, this could be triggered by the pH-regulated adenylate cyclase producing elevated levels of cyclic AMP (cAMP) to activate cAMP-receptor protein (22), a transcriptional regulator of the mycobacterial respiratory chain (23–25). Activated cAMP-receptor protein would then lower the expression of respiratory chain complexes, providing a potential mechanism for the decreased respiration and capacity in the Δ*mqo* mutant compared to the WT (24, 25).

Intracellular accumulation of fumarate has been shown in mycobacteria to cause toxicity through succination of metabolites with thiol groups, such as cysteine and mycothiol (MSH) (26). Therefore, we measured the levels of succinocystine and succinated MSH and found that there was an average log2-fold increase of 8 and 4 in the Δ*mqo* mutant relative to WT, respectively (Fig. 4). With MSH being a major mechanism for mycobacterial oxidative stress mitigation, the increase in succinated MSH suggests the Δ*mqo* mutant may be less tolerant to oxidative stress as has been previously observed in a fumarase mutant in *M. tuberculosis* (26). This idea would be consistent with the slow growth rates observed on aerobic substrates and the reduced respiratory capacity in the *M. smegmatis* Δ*mqo* mutant.

Mdh from M. tuberculosis *can compensate for loss of Mqo function in* M. smegmatis

To explore the degree to which Mqo and Mdh are functionally redundant in mycobacteria and making use of the fact that *M. smegmatis* harbors only *mqo*, we examined whether the Δ*mqo* mutant could be complemented with a copy of *mdh* from *M. tuberculosis*. Therefore, we created two genetic constructs, one to express *M. smegmatis mqo* (pMqoMS) and the other to express *M. tuberculosis mdh* (pMdhTB). We found that both pMqoMS and pMdhTB resulted in complete restoration of the Δ*mqo* mutant to WT growth kinetics on the fermentable carbon sources glycerol (Fig. 5*A*) and glucose (Fig. 5*B*) compared to the impaired growth observed with the empty vector control (pMind) (Fig. 5, *A* and *B*). When pMqoMS and pMdhTB were used for complementation on the nonfermentable carbon sources malate (Fig. 5*C*) and succinate (Fig. 5*D*), pMqoMS restored growth to WT levels on both carbon sources. Growth was delayed with pMdhTB, but after 20 h incubation, cells grew at growth rates like the WT (Fig. 5, *C* and *D*). No growth was observed in the Δ*mqo* pMind mutant background, and pMind has no effect on growth of the WT (Fig. 5, *C* and *D*). Previous work demonstrated that the addition of the vitamin nicotinamide could partially restore the growth of a *C. glutamicum mqo* mutant, but not in a mutant lacking both Mqo and Mdh, suggesting Mdh can substitute for Mqo when nicotinamide is provided in the growth medium (6). When nicotinamide was included in our growth medium,

to WT (*blue circles*) grown on HdB minimal medium with glycerol (22 mM). *G*, concentration of malate in the cell-free supernatant of bacterial cultures (Δ*mqo* mutant and WT) grown in panel *F*. Samples were taken from stationary phase cultures for malate concentration determinations. All reported measurements are an average of biological triplicates with error bars representing standard deviation. CCCP, carbonyl cyanide *m*-chlorophenyl hydrazine.

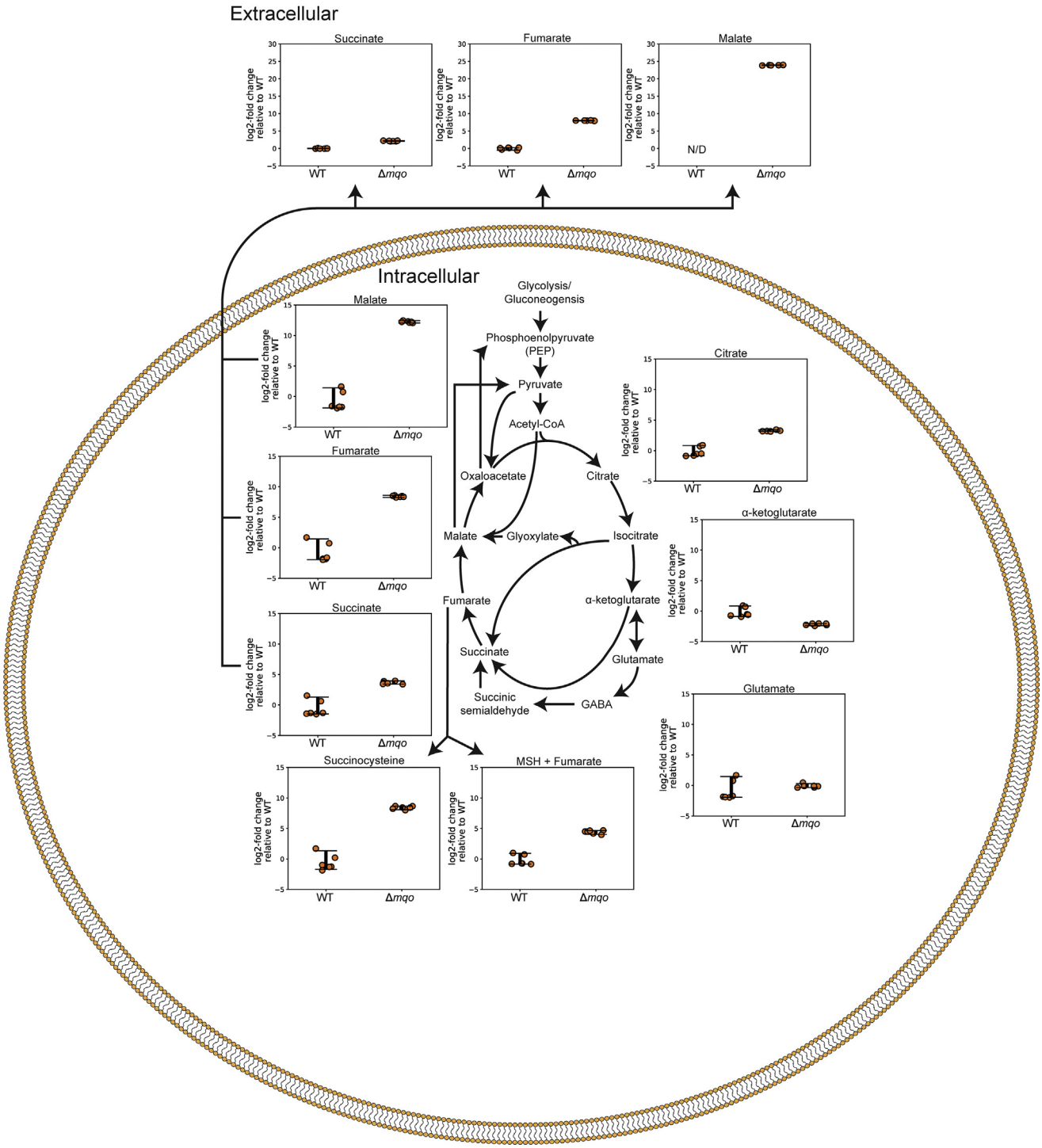

Figure 4. Metabolic consequences of impaired malate oxidation in *M. smegmatis*. Comparison of selected intracellular and extracellular metabolites between the Δ*mqo* mutant and WT *M. smegmatis* after 24 h incubation of bacteria-laden filters on plates containing Middlebrook 7H9 liquid broth with 0.2% glycerol (see Experimental procedures). Schematic of TCA cycle components of mycobacteria. Data values shown represent log2-fold change of biological duplicate with technical triplicate with error bars representing 95% confidence interval. All intracellular metabolite abundances were first normalized to a single reference intracellular compound (glycerol 3-phosphate) before computing log2-fold changes relative to average WT strain abundances. When no extracellular metabolites were detected for a strain, log2-fold change analyzed was relative to 1. TCA, tricarboxylic acid.

we observed no effect on the growth of either the WT or the Δ*mqo* mutant on either malate or succinate, and no stimulation of complementation with Mdh in the Δ*mqo* background was observed indicating that nicotinamide was without effect in *M. smegmatis* (Fig. 5, *C* and *D*).

Mdh or Mqo can drive malate oxidation in M. tuberculosis*, but growth is severely impaired when both are absent*

To determine the role of Mqo and Mdh in *M. tuberculosis*, we used CRISPR interference to systematically knockdown the expression of either *mqo* and/or *mdh* under selected growth

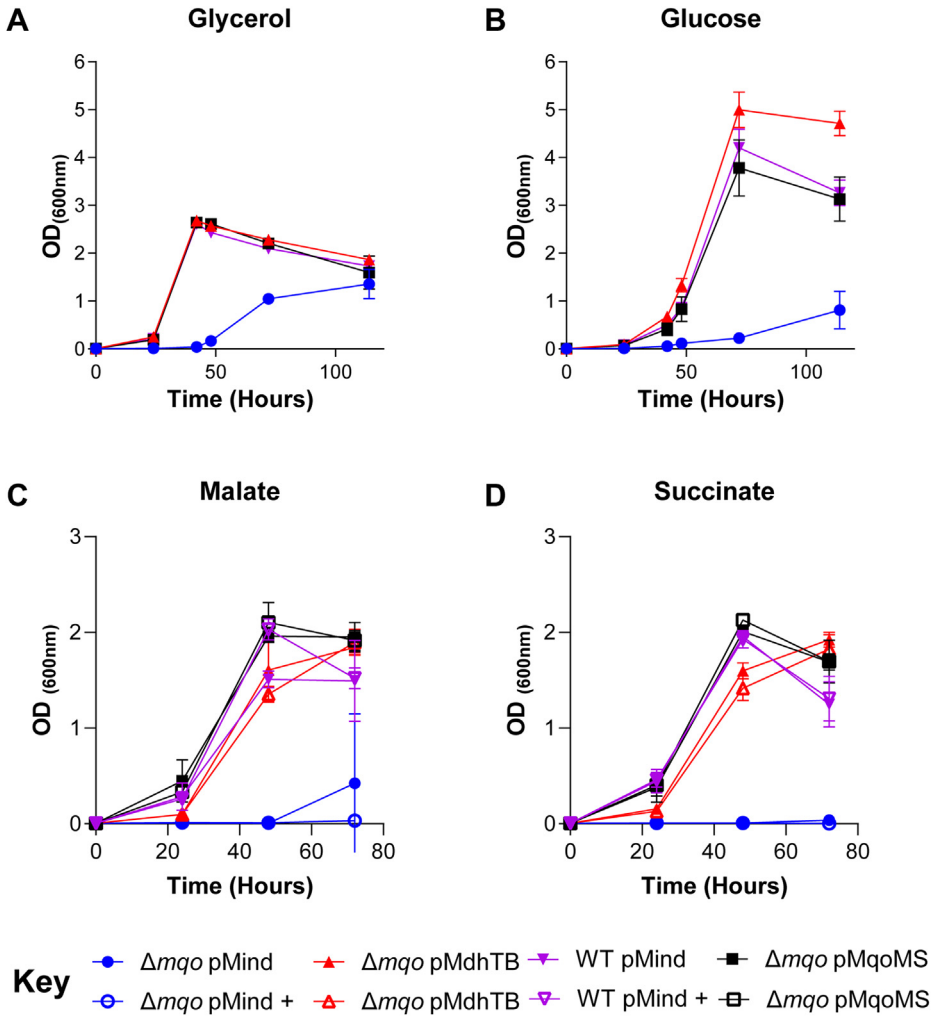

Figure 5. Complementation of *M. smegmatis* Δ*mqo* mutant with either pMqoMS or pMdhTB restores growth on nonfermentable carbon sources. Growth of the *M. smegmatis* Δ*mqo* mutant complemented with pMind empty vector control (*solid blue circles*), pMqoMS (*M. smegmatis* Mqo, *solid black squares*), pMdhTB (*M. tuberculosis* Mdh, *solid red triangles*) compared to WT with pMind empty vector control (*solid purple inverted triangles*) on HdB minimal medium with the following carbon sources: *A*, glycerol (20 mM); *B*, glucose (20 mM); *C*, malate (20 mM); *D*, succinate (20 mM) as the sole carbon and energy source. In panels (*C*) and (*D*), nicotinamide (1 mg/l) was included in the growth medium (all open symbols). All growth (A_{600}) measurements are an average of biological triplicate with error bars representing standard deviation.

conditions (27, 28). We tested single and double transcriptional knockdowns of *mqo* and *mdh* in *M. tuberculosis*, along with a positive control *mmpL3* essential gene knockdown and an untargeted negative control. We first confirmed that all the single guide RNA (sgRNA) molecules targeting constructs were successfully inhibiting transcription of their respective target genes. Using RT-qPCR and RNA extracted from cells grown in Middlebrook 7H9 broth (Fig. 6, *A* and *B*), we found that relative to the nontargeted sgRNA negative control, the *mqo* single knockdown resulted in an average of 226-fold repression, while the *mdh* single knockdown caused an average of 345-fold repression (Fig. 6, *A* and *B*). The double knockdown of both *mqo* and *mdh* resulted in an average 232-fold repression of *mqo* and 174-fold repression of *mdh* (Fig. 6, *A* and *B*). Neither of the *mqo* or *mdh* single knockdowns displayed any evidence of upregulation to compensate for the depletion of the alternative gene (Fig. 6, *A* and *B*). Overall, these data indicated that we were able to effectively knockdown the expression of either *mqo*, *mdh*, or both in combination in *M. tuberculosis*.

To examine the effect of the single and double knockdowns of either *mqo* and/or *mdh* on *M. tuberculosis* physiology, we grew cultures with each of the different knockdown constructs on 7H9 media with either glucose or succinate as the primary carbon source representing fermentable and nonfermentable substrates, respectively (Fig. 6, *C* and *D*). Knockdown of the essential gene *mmpL3* showed no growth under the experimental conditions used here as previously reported (Fig. 6, *C* and *D*) (27). We found that on both carbon sources, knockdown of either *mqo* or *mdh* resulted in delayed and slower growth compared to the scrambled nontargeted sgRNA control (Fig. 6, *C* and *D*). Knockdown of both *mqo* and *mdh* in combination on either carbon source resulted in a more severe growth defect compared to the nontargeted sgRNA control and the individual gene *mqo* and *mdh* knockdowns (Fig. 6, *C* and *D*). When we evaluated the specific growth rate of *M. tuberculosis* between days 0 and 6, we found that transcriptional knockdown of either *mqo* or *mdh* causes slower growth rates compared to the nontargeted sgRNA control, and

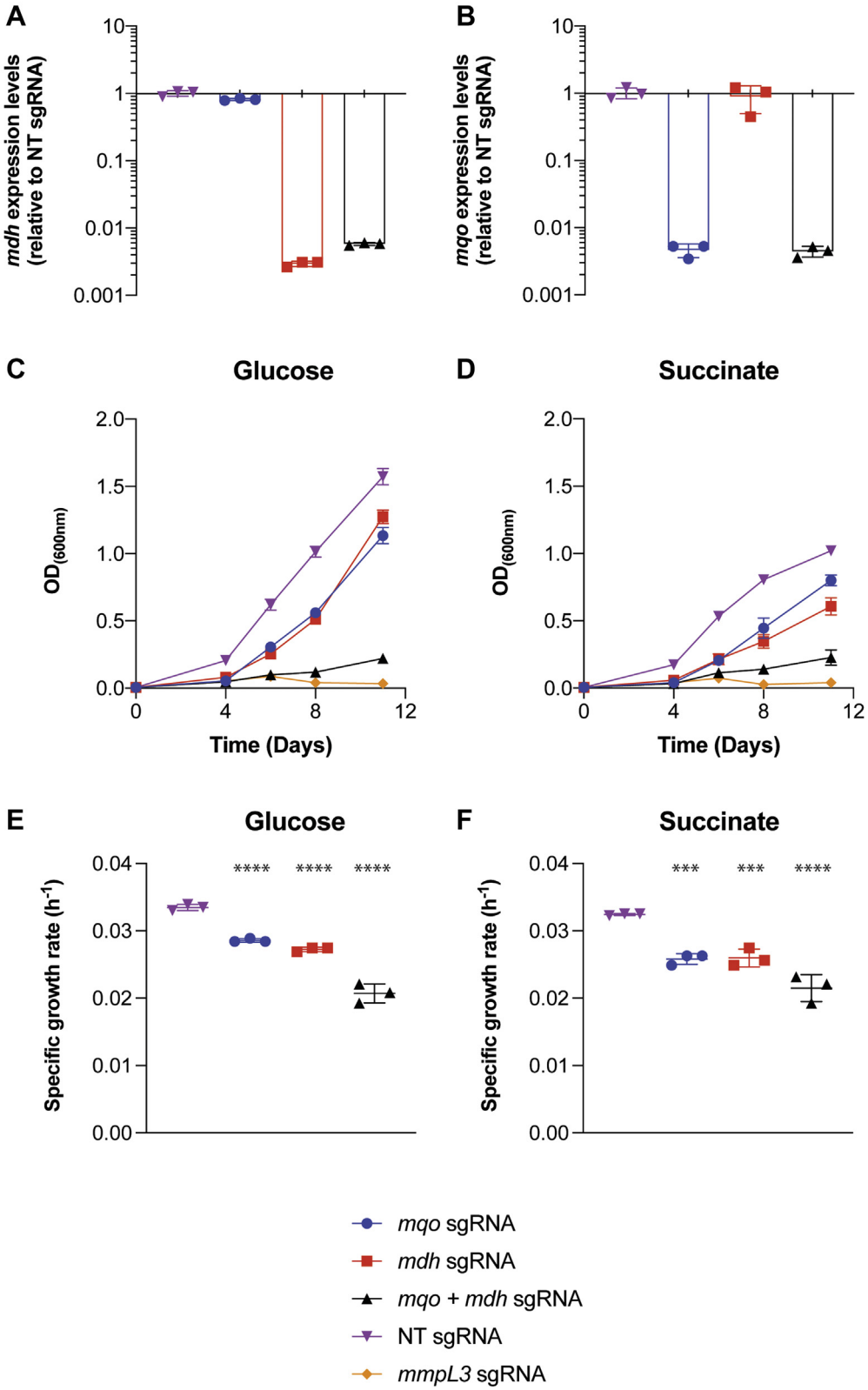

Figure 6. Mdh and Mqo both contribute to optimal malate oxidation in *M. tuberculosis*. Relative expression (mRNA levels) of *mdh* (*A*) and *mqo* (*B*) with different CRISPRi knockdown single guide RNA (sgRNA) molecules targeting *mqo* (*blue circles*), *mdh* (*red squares*) and a combination of both (*black triangles*). The mRNA levels of *mdh* and *mqo* are expressed relative to a scrambled nontargeted (NT) sgRNA control (*purple inverted triangles*). Gene knockdowns were initiated by the addition of 300 ng/ml (final concentration) anhydrotetracycline. RT-qPCR values are an average of a technical triplicate with error bars representing standard deviation. *C* and *D*, growth of *M. tuberculosis strain* $mc^2$6230 on Middlebrook 7H9 base medium with either 0.2% glucose (*C*) or 30 mM succinate (*D*) as the sole carbon and energy source with sgRNA molecules targeting; *mqo* (*blue circles*), *mdh* (*red squares*), and a combination of both (*black triangles*). An *mmpL3*-targeting sgRNA (*yellow diamonds*) was used as a positive control and a nontargeted sgRNA (*purple inverted triangles*) as a negative control. *E* and *F*, specific growth rate (h^{-1}) of all strains determined from the A_{600} values at days 0 and 6 with a one-way ANOVA with Dunnett's multiple comparisons to the NT sgRNA. ***$p < 0.001$, ****$p < 0.0001$. Measurements are an average of biological triplicate with error bars representing standard deviation. Mdh, malate dehydrogenase; Mqo, malate quinone oxidoreductase.

the transcriptional knockdown of both had an additive effect resulting in a slower growth rate than the single knockdowns alone (Fig. 6, *E* and *F*). These data show that either Mqo or Mdh can be used to effectively catalyze oxidation of malate in *M. tuberculosis*, but the growth rate is reduced compared to cells expressing both enzymes illustrating there is incomplete functional redundancy. Moreover, simultaneous knockdown of *mqo* and *mdh* severely limits growth, even on fermentable carbon sources demonstrating that both enzymes are required for optimal growth of *M. tuberculosis*.

Rittershaus *et al.* (29) demonstrated that Mdh is required for the metabolism and survival of *M. tuberculosis in vitro* and *in vivo*. Moreover, chemical inhibitors of *M. tuberculosis* Mdh had the ability to inhibit growth and rapidly kill hypoxic quiescent cells (nonreplicating) *in vitro* and during infection of the murine lung (29). Based on our data, we propose that the addition of an inhibitor of Mqo, in combination with Mdh inhibitors, may enhance the growth inhibition of *M. tuberculosis* further while still retaining potent activity against nonreplicating populations. In this regard, Mqo is not found in mammalian cells, and potent inhibitors have been reported that target the mitochondrial malate:quinone oxidoreductase of the malarial parasite *Plasmodium falciparum* (30). The significant structural differences reported between the human and mycobacterial Mdh enzymes (29) suggest a combination therapy of Mqo and Mdh inhibitors may be attractive for tuberculosis drug development.

Conclusions

Central carbon metabolism is regarded as a focal point in mycobacterial metabolism with various pathways being identified as vulnerable targets (10, 17, 21, 26, 31). We report that Mqo is widely prevalent in bacteria, and in mycobacteria, Mqo is favored over Mdh. When the *mqo* gene of *M. smegmatis* was deleted, it caused severe growth phenotypes, succination of metabolites and an accumulation of intracellular and extracellular malate. *M. tuberculosis mdh* was able to functionally complement *mqo* in *M. smegmatis* on nonfermentable carbon sources. In *M. tuberculosis* when either *mqo* or *mdh* was depleted, there was a slower growth rate compared to the nontargeted sgRNA control, which was lowered further when both enzymes were depleted in combination. Taken together, these data illustrate that Mqo is critical for optimal growth and carbon metabolism in mycobacteria, and disruption of malate oxidation causes significant alteration to central carbon metabolism. In *M. tuberculosis*, it has been shown that Mdh is critical to its survival during periods of hypoxia due to the need drive reductive TCA cycle activity (29). Our data indicate that in addition to using Mdh for reductive TCA under hypoxia, *M. tuberculosis* can use Mdh for oxidation of malate during aerobic growth if Mqo is absent.

Experimental procedures

Bacterial strains and plasmids

All bacteria, strains and plasmids used in this study are listed in Table S1. *E. coli* used for cloning and plasmid amplification were grown on Luria–Bertani medium at 37 °C with appropriate antibiotics. All molecular biology techniques were carried out according to the manufacturer's procedures. All restriction enzymes and DNA modifying enzymes used were from New England Biolabs and were used in their appropriate buffers. *M. smegmatis* strain mc^{2}155 (32) and derived strains were routinely grown at 37 °C in Luria–Bertani containing 0.05% (w/v) Tween 80 or in modified Hartman's de Bont medium (33), containing 0.2% glycerol (v/v) as the sole carbon and energy source. For *M. tuberculosis* strain mc^{2}6230 growth (Table S1), cells were grown in Middlebrook 7H9 broth supplemented with OADC (0.005% oleic acid, 0.5% bovine serum albumin, 0.2% dextrose, 0.085% catalase), 0.05% tyloxapol (Sigma) and 25 μg/ml pantothenic acid. Unless otherwise specified, the following growth procedures were followed: *M. smegmatis* was grown in 125 ml conical flasks, containing 25 ml media, and *M. tuberculosis* was grown in 30 ml inkwells, containing 10 ml growth media. *M. smegmatis* and *M. tuberculosis* were grown with agitation at 200 rpm and 140 rpm respectively. All cultures were maintained at 37 °C. Growth was monitored by following the absorbance at 600 nm using a Jenway 6300 spectrophotometer.

Marked deletion mutant construction and complementation

The initial construct for creating a marked deletion of *mqo* was made by amplifying homologous regions either side of the *mqo* gene using the primers LH21, LH22, LH23, and LH24 (Table S2). Following this, the remainder of the deletion method was carried out as described by Jain *et al.* (34). Hygromycin-resistant (Hyg^R) colonies were indicative of a successful double homologous recombination with the gene being replaced with Hyg^R-*sacB* DNA fragment. Successful marked (Hyg^R) deletion mutants were confirmed using whole genome sequencing and enzymatic activity assays. The complementation constructs used to express Mqo and Mdh were created in the pMind vector backbone (35) with an artificial ribosome binding site (36, 37) with the primers LH25 and LH26 used to amplify Mqo and LH27 and LH28 used to amplify Mdh from *M. smegmatis* and *M. tuberculosis*, respectively (Table S2). The vectors were designated pMqoMS and pMdhTB. Leaky gene expression from the pMind vector was sufficient for complementation, and no tetracycline was added. When *M. smegmatis* was grown with either of these plasmids or an empty vector control, the growth media was supplemented with 20 μg/ml kanamycin (final concentration). To determine the effect of nicotinamide on growth, nicotinamide was added to the growth medium at 1 mg/l according to Molenaar *et al.* (6).

Comparative metabolomics and data analysis

Metabolomics was performed as previously described (38, 39). Two independent cultures of *M. smegmatis* WT and the Δ*mqo* mutant were grown overnight at 37 °C in 7H9 medium (Middlebrook 7H9 broth supplemented with 0.2% glycerol, 0.5% BSA fraction, 0.085% NaCl, and 0.05% Tyloxapol). Outgrowth cultures were diluted into fresh 7H9 media

without Tyloxapol. Culture (1 ml, A_{600} = 1.0) was filtered through a 0.22 μM Durapore membrane filter. Filters were placed overnight at 37 °C on 7H10 agar media. Filters were then placed on top of plates filled with 3 ml of 7H9 medium (no Tyloxapol). After 24 h, filters were quenched in tubes containing zirconium beads immersed in a 1 ml cooled mixture of acetonitrile, methanol, and water (2:2:1 ratio). Bacteria were lysed by bead-beating (six times at 6000 RPM). Extracts were filtered through a 0.22 μM Spin X columns (Corning). To measure secreted metabolites, 200 μl of remaining media was collected from the plates into a mixture of acetonitrile (400 μl) and methanol (400 μl). For MS analysis, samples were mixed in a 1:1 ratio of acetonitrile and 0.2% formic acid and analyzed on an Agilent Accurate Mass 6220 TOF system coupled to an Agilent 1200 LC system using a Cogent Diamond hybrid type C column (Microsolve Technologies). Extracted ion chromatograms and metabolite abundances were obtained using Agilent ProFinder software tool in batch targeted analysis mode (parameter details). Raw metabolite abundances obtained with ProFinder were exported into tabular format and further analyzed with an in-house Python script. All intracellular metabolite abundances were first normalized to a single reference intracellular compound, glycerol 3-phosphate before computing log2-fold changes relative to average WT strain abundances. The concentration of malate from cell-free supernatants was measured using a malate colorimetric assay kit from Sigma according to the manufacturer's instructions. The percentage of total carbon was calculated by converting the concentration measurements into the number of molecules and then calculating the percentage, while adjusting for the number of carbon atoms in each molecule.

M. tuberculosis *gene knockdowns using CRISPRi and qPCR*

The single knockdown CRISPRi sgRNA constructs were created as previously described using the primers Mqo_TBF plus Mqo_TBR and Mdh_TBF plus Mdh_TBR (27, 40) (Table S2). Plasmid containing clones were then sequenced using the DNA sequencing primers MMO117 plus MMO119 and named pCi118 (*mqo*) and pCi120 (*mdh*) (Table S2). For double sgRNA knockdown constructs, the *mqo* targeting spacer, promoter, and repeats from pCi118 were amplified using the primers MMO120 plus MMO121 and cloned into pCi120 using SapI golden gate cloning (27) to create pCiMX164 (*mdh* plus *mqo*) (Tables S1 and S2). The *M. tuberculosis* strain $mc^2$6230 was used in all gene knockdown experiments (41) (Table S1). The medium for the knockdown experiments was Middlebrook 7H9 broth supplemented with OADC, pantothenate (25 μg/ml), kanamycin (25 μg/ml), and tyloxapol (0.05%). Alternatively, the OADC was replaced with BSA (0.5%) and NaCl (0.09%), and the desired carbon source, *i.e.*, glucose (11 mM) or succinate (30 mM). Gene knockdowns were initiated by the addition of 300 ng/ml (final concentration) anhydrotetracycline.

For qPCR analysis, *M. tuberculosis* strains were grown with 300 ng/ml anhydrotetracycline for 3 days and harvested by centrifugation at 3126*g*. RNA was extracted from cells and converted to cDNA as previously described (27, 40). qPCR reactions were performed in 96-well or 384-well plates using Invitrogen PowerUp SYBR Green Master Mix in a ViiA7 Thermocycler with 3 μl of 1/100 dilution of the cDNA (27). The *mqo* (MqoF plus MqoR), *mdh* (MdhF plus MdhR), and *sigA* (MMO173 plus MMO 174) gene abundances were measured with their respective primer pairs at 500 nM (Table S2). Signals were normalized to the housekeeping *sigA* transcript and quantified by the 2ΔΔCt method (27).

Oxygen consumption, Mqo, and Mez activity measurements

To determine whole cell OCRs, growing cells on selected carbon sources were harvested and washed with MRA buffer (158 mM NaCl, 5.4 mM KCl, 15 mM $[NH_4]_2SO_4$, HdB trace metals (33), 0.05% tween 80). Washed cells suspensions were normalized to an absorbance (600 nm) of 0.5 or 1.0 in MRA buffer. Washed cells (2 ml) were pipetted into the high-resolution Oroboros Oxygraphy-2k (polarographic oxygen sensor) before being sealed and respiration initiated by the addition of the designated carbon source. Total protein concentration of cells was determined using the BCA assay (Sigma) with bovine serum albumin as the standard. Oxygen consumption was normalized to protein concentration and reported as nmol O_2 consumed min^{-1} mg protein-1. Cells were uncoupled using the protonophore CCCP (5 μM) to achieve maximal rates of respiration in the absence of respiratory back pressure (19, 20).

Mqo activity linked to respiratory chain activity (proton pumping) was assayed using IMVs and ACMA quenching as previously described (17, 20). The reaction was then initiated by adding either succinate or malate as the electron donor. Once the fluorescence quenching reached a steady state, the proton gradient was collapsed by the addition of the uncoupler CCCP. The excitation and emission wavelengths were 493 and 530 nm, respectively.

For oxygen consumption measurements using IMVs, 0.5 mg of IMVs was added to 2 ml of buffer (50 mM Tris-HCl, pH 7.5) into the Oroboros Oxygraphy-2k chamber. Oxygen consumption was initiated with either 100 μM NADH or 3.5 mM malate (final concentration). For Mqo activity measurements, IMVs were incubated at 37 °C in (1 ml) 50 mM Tris-SO_4 (pH 7.5) with 66 μl 0.33% (w/v) phenazine ethosulfate and 34 μl 0.05% (w/v) DCIP. The reaction was then initiated by the addition of 7 mM malate (final concentration). The reduction of DCIP was followed by measuring the absorbance at 600 nm of DCIP using an extinction coefficient of 19.1 mM^{-1} cm^{-1} with an Evolution 260 bio spectrophotometer (Thermo Fisher). For Mez-like activity, the cytosolic fraction from the IMVs preparation was used and incubated in 50 mM Tris-SO_4 (pH 7.5) with 10 mM malate. The reaction was initiated by the addition of 200 μM $NADP^+$ followed by measuring absorbance at 340 nm with an Evolution 260 bio spectrophotometer (Thermo Fisher).

Bioinformatic search for Mqo and Mdh across bacterial proteomes

To search for either the presence or absence of Mqo and Mdh genes within mycobacterial species, we used the

phylogenetic tree of Fedrizzi *et al.* (42). The species in the mycobacterial phylogeny were mapped onto UniProt proteome IDs, and proteome annotations were searched for the presence or absence of Mqo and Mdh. Specifically, proteins annotated with the Enzyme Commission (EC) number 1.1.5.4 were flagged as having Mqo, while those annotated with EC number 1.1.1.37 were flagged as having Mdh. To validate the accuracy of our presence/absence calls, we performed a protein sequence–based search of Mqo and Mdh for all "negative" cases (samples lacking Mqo or Mdh according to the EC number analysis) using BLAST (43). The *M. tuberculosis* Mqo and Mdh protein sequences were used as queries, and we performed a BLAST search (E-value threshold = 0.01.) against each mycobacterial proteomes. To analyze of presence or absence of *mdh* and *mqo* genes across a wider set of bacterial species, we obtained the set of UniProt *reference* bacterial proteomes, which are selected both manually and algorithmically by UniProt as "landmarks in proteome space" to "provide broad coverage of the tree of life" (44). After discarding "environmental" proteomes with no taxonomic labels, we performed the analysis on a final set of 6240 bacterial reference proteomes. Visual representations of phylogenies with surrounding color-coded rings were generated using the software tool GraPhlAn (45).

Data availability

All data are contained within the manuscript and the supplementary information file.

Supporting information—This article contains supporting information (28, 32, 34, 35, 41).

Author contributions—L. K. H., A. J., K. R., and G. M. C. conceptualization; L. K. H. and A. J. data curation; L. K. H. and A. J. formal analysis; L. K. H., A. J., K. H., Alexandra Cordeiro, Alec Cross, M. B. M., and L. M. K. investigation; L. K. H., A. J., K. H., Alexandra Cordeiro, Alec Cross, M. B. M., G. M. C., and L. M. K. methodology; L. K. H., A. J., K. R., and G. M. C. project administration; L. K. H., A. J., K. R., and G. M. C. supervision; A. J., L. K. H., M. B. M., G. M. C., K. R., and K. H. writing-original draft; L. K. H. and G. M. C. writing-review & editing; K. R. and G. M. C. funding acquisition.

Funding and additional information—This work was financially supported by the Maurice Wilkins Centre for Molecular Biodiscovery and the Marsden Fund, Royal Society of New Zealand. A. J. was supported by a Hanna Gray Fellowship, Howard Hughes Medical Institute.

Conflict of interest—The authors declare that they have no conflicts of interest with the contents of this article.

Abbreviations—The abbreviations used are: ACMA, 9-amino-6-chloro-2-methoxyacridine; cAMP, cyclic AMP; CCCP, carbonyl cyanide *m*-chlorophenyl hydrazine; DCIP, 2,6 dichlorophenolindophenol; IMVs, inverted membrane vesicles; Mdh, malate dehydrogenase; Mez, malic enzyme; Mqo, malate quinone oxidoreductase; MSH, mycothiol; OCR, oxygen consumption rate; sgRNA, single guide RNA; TCA, tricarboxylic acid.

References

1. Mailloux, R. J., Beriault, R., Lemire, J., Singh, R., Chenier, D. R., Hamel, R. D., and Appanna, V. D. (2007) The tricarboxylic acid cycle, an ancient metabolic network with a novel twist. *PLoS One* **2**, e690
2. Gourdon, P., Baucher, M. F., Lindley, N. D., and Guyonvarch, A. (2000) Cloning of the malic enzyme gene from *Corynebacterium glutamicum* and role of the enzyme in lactate metabolism. *Appl. Environ. Microbiol.* **66**, 2981–2987
3. Mogi, T., Murase, Y., Mori, M., Shiomi, K., Omura, S., Paranagama, M. P., and Kita, K. (2009) Polymyxin B identified as an inhibitor of alternative NADH dehydrogenase and malate: Quinone oxidoreductase from the Gram-positive bacterium *Mycobacterium smegmatis*. *J. Biochem.* **146**, 491–499
4. van der Rest, M. E., Frank, C., and Molenaar, D. (2000) Functions of the membrane-associated and cytoplasmic malate dehydrogenases in the citric acid cycle of *Escherichia coli*. *J. Bacteriol.* **182**, 6892–6899
5. Molenaar, D., van der Rest, M. E., and Petrovic, S. (1998) Biochemical and genetic characterization of the membrane-associated malate dehydrogenase (acceptor) from *Corynebacterium glutamicum*. *Eur. J. Biochem.* **254**, 395–403
6. Molenaar, D., van der Rest, M. E., Drysch, A., and Yucel, R. (2000) Functions of the membrane-associated and cytoplasmic malate dehydrogenases in the citric acid cycle of *Corynebacterium glutamicum*. *J. Bacteriol.* **182**, 6884–6891
7. Thauer, R. K., Jungermann, K., and Decker, K. (1977) Energy conservation in chemotrophic anaerobic bacteria. *Bacteriol. Rev.* **41**, 100–180
8. Wu, F., and Minteer, S. (2015) Krebs cycle metabolon: Structural evidence of substrate channeling revealed by cross-linking and mass spectrometry. *Angew. Chem. Int. Ed. Engl.* **54**, 1851–1854
9. Wang, Q., Yu, L., and Yu, C. A. (2010) Cross-talk between mitochondrial malate dehydrogenase and the cytochrome bc1 complex. *J. Biol. Chem.* **285**, 10408–10414
10. Hards, K., Adolph, C., Harold, L. K., McNeil, M. B., Cheung, C. Y., Jinich, A., Rhee, K. Y., and Cook, G. M. (2020) Two for the price of one: Attacking the energetic-metabolic hub of mycobacteria to produce new chemotherapeutic agents. *Prog. Biophys. Mol. Biol.* **152**, 35–44
11. Tian, J., Bryk, R., Itoh, M., Suematsu, M., and Nathan, C. (2005) Variant tricarboxylic acid cycle in Mycobacterium tuberculosis: Identification of -ketoglutarate decarboxylase. *Proc. Natl. Acad. Sci. U. S. A.* **102**, 10670–10675
12. Watanabe, S., Zimmermann, M., Goodwin, M. B., Sauer, U., Barry, C. E., 3rd, and Boshoff, H. I. (2011) Fumarate reductase activity maintains an energized membrane in anaerobic *Mycobacterium tuberculosis*. *PLoS Pathog.* **7**, e1002287
13. Berney, M., Greening, C., Conrad, R., Jacobs, W. R., Jr., and Cook, G. M. (2014) An obligately aerobic soil bacterium activates fermentative hydrogen production to survive reductive stress during hypoxia. *Proc. Natl. Acad. Sci. U. S. A.* **111**, 11479–11484
14. Berney, M., and Cook, G. M. (2010) Unique flexibility in energy metabolism allows mycobacteria to combat starvation and hypoxia. *PLoS One* **5**, e8614
15. Greening, C., Berney, M., Hards, K., Cook, G. M., and Conrad, R. (2014) A soil actinobacterium scavenges atmospheric H_2 using two membrane-associated, oxygen-dependent [NiFe] hydrogenases. *Proc. Natl. Acad. Sci. U. S. A.* **111**, 4257–4261
16. Vilcheze, C., Weisbrod, T. R., Chen, B., Kremer, L., Hazbon, M. H., Wang, F., Alland, D., Sacchettini, J. C., and Jacobs, W. R., Jr. (2005) Altered NADH/NAD+ ratio mediates coresistance to isoniazid and ethionamide in mycobacteria. *Antimicrob. Agents Chemother.* **49**, 708–720
17. Pecsi, I., Hards, K., Ekanayaka, N., Berney, M., Hartman, T., Jacobs, W. R., Jr., and Cook, G. M. (2014) Essentiality of succinate dehydrogenase in *Mycobacterium smegmatis* and its role in the generation of the membrane potential under hypoxia. *mBio* **5**, e01093-14

18. Basu, P., Sandhu, N., Bhatt, A., Singh, A., Balhana, R., Gobe, I., Crowhurst, N. A., Mendum, T. A., Gao, L., Ward, J. L., Beale, M. H., McFadden, J., and Beste, D. J. V. (2018) The anaplerotic node is essential for the intracellular survival of Mycobacterium tuberculosis. *J. Biol. Chem.* **293**, 5695–5704
19. Lamprecht, D. A., Finin, P. M., Rahman, M. A., Cumming, B. M., Russell, S. L., Jonnala, S. R., Adamson, J. H., and Steyn, A. J. (2016) Turning the respiratory flexibility of Mycobacterium tuberculosis against itself. *Nat. Commun.* **7**, 12393
20. Hards, K., Robson, J. R., Berney, M., Shaw, L., Bald, D., Koul, A., Andries, K., and Cook, G. M. (2015) Bactericidal mode of action of bedaquiline. *J. Antimicrob. Chemother.* **70**, 2028–2037
21. Puckett, S., Trujillo, C., Wang, Z., Eoh, H., Ioerger, T. R., Krieger, I., Sacchettini, J., Schnappinger, D., Rhee, K. Y., and Ehrt, S. (2017) Glyoxylate detoxification is an essential function of malate synthase required for carbon assimilation in *Mycobacterium tuberculosis*. *Proc. Natl. Acad. Sci. U. S. A.* **114**, E2225–E2232
22. Tews, I., Findeisen, F., Sinning, I., Schultz, A., Schultz, J. E., and Linder, J. U. (2005) The structure of a pH-sensing mycobacterial adenylyl cyclase holoenzyme. *Science* **308**, 1020–1023
23. Rickman, L., Scott, C., Hunt, D. M., Hutchinson, T., Menendez, M. C., Whalan, R., Hinds, J., Colston, M. J., Green, J., and Buxton, R. S. (2005) A member of the cAMP receptor protein family of transcription regulators in *Mycobacterium tuberculosis* is required for virulence in mice and controls transcription of the *rpfA* gene coding for a resuscitation promoting factor. *Mol. Microbiol.* **56**, 1274–1286
24. Aung, H. L., Berney, M., and Cook, G. M. (2014) Hypoxia-activated cytochrome *bd* expression in *Mycobacterium smegmatis* is cyclic AMP receptor protein dependent. *J. Bacteriol.* **196**, 3091–3097
25. Aung, H. L., Dixon, L. L., Smith, L. J., Sweeney, N. P., Robson, J. R., Berney, M., Buxton, R. S., Green, J., and Cook, G. M. (2015) Novel regulatory roles of cAMP receptor proteins in fast-growing environmental mycobacteria. *Microbiology* **161**, 648–661
26. Ruecker, N., Jansen, R., Trujillo, C., Puckett, S., Jayachandran, P., Piroli, G. G., Frizzell, N., Molina, H., Rhee, K. Y., and Ehrt, S. (2017) Fumarase deficiency causes protein and metabolite succination and intoxicates *Mycobacterium tuberculosis*. *Cell Chem. Biol.* **24**, 306–315
27. McNeil, M. B., and Cook, G. M. (2019) Utilization of CRISPR interference to validate MmpL3 as a drug target in *Mycobacterium tuberculosis*. *Antimicrob. Agents Chemother.* **63**, e00629-19
28. Rock, J. M., Hopkins, F. F., Chavez, A., Diallo, M., Chase, M. R., Gerrick, E. R., Pritchard, J. R., Church, G. M., Rubin, E. J., Sassetti, C. M., Schnappinger, D., and Fortune, S. M. (2017) Programmable transcriptional repression in mycobacteria using an orthogonal CRISPR interference platform. *Nat. Microbiol.* **2**, 16274
29. Rittershaus, E. S. C., Baek, S. H., Krieger, I. V., Nelson, S. J., Cheng, Y. S., Nambi, S., Baker, R. E., Leszyk, J. D., Shaffer, S. A., Sacchettini, J. C., and Sassetti, C. M. (2018) A lysine acetyltransferase contributes to the metabolic adaptation to hypoxia in *Mycobacterium tuberculosis*. *Cell Chem. Biol.* **25**, 1495–1505.e3
30. Hartuti, E. D., Inaoka, D. K., Komatsuya, K., Miyazaki, Y., Miller, R. J., Xinying, W., Sadikin, M., Prabandari, E. E., Waluyo, D., Kuroda, M., Amalia, E., Matsuo, Y., Nugroho, N. B., Saimoto, H., Pramisandi, A., *et al.* (2018) Biochemical studies of membrane bound Plasmodium falciparum mitochondrial L-malate:quinone oxidoreductase, a potential drug target. *Biochim. Biophys. Acta Bioenerg.* **1859**, 191–200
31. Eoh, H., and Rhee, K. Y. (2013) Multifunctional essentiality of succinate metabolism in adaptation to hypoxia in *Mycobacterium tuberculosis*. *Proc. Natl. Acad. Sci. U. S. A.* **110**, 6554–6559
32. Snapper, S. B., Melton, R. E., Mustafa, S., Kieser, T., and Jacobs, W. R., Jr. (1990) Isolation and characterization of efficient plasmid transformation mutants of *Mycobacterium smegmatis*. *Mol. Microbiol.* **4**, 1911–1919
33. Berney, M., Weimar, M. R., Heikal, A., and Cook, G. M. (2012) Regulation of proline metabolism in mycobacteria and its role in carbon metabolism under hypoxia. *Mol. Microbiol.* **84**, 664–681
34. Jain, P., Hsu, T., Arai, M., Biermann, K., Thaler, D. S., Nguyen, A., Gonzalez, P. A., Tufariello, J. M., Kriakov, J., Chen, B., Larsen, M. H., and Jacobs, W. R., Jr. (2014) Specialized transduction designed for precise high-throughput unmarked deletions in *Mycobacterium tuberculosis*. *mBio* **5**, e01245-14
35. Blokpoel, M. C., Murphy, H. N., O'Toole, R., Wiles, S., Runn, E. S., Stewart, G. R., Young, D. B., and Robertson, B. D. (2005) Tetracycline-inducible gene regulation in mycobacteria. *Nucleic Acids Res.* **33**, e22
36. Robson, J., McKenzie, J. L., Cursons, R., Cook, G. M., and Arcus, V. L. (2009) The *vapBC* operon from *Mycobacterium smegmatis* is an autoregulated toxin-antitoxin module that controls growth via inhibition of translation. *J. Mol. Biol.* **390**, 353–367
37. Harold, L. K., Antoney, J., Ahmed, F. H., Hards, K., Carr, P. D., Rapson, T., Greening, C., Jackson, C. J., and Cook, G. M. (2019) FAD-sequestering proteins protect mycobacteria against hypoxic and oxidative stress. *J. Biol. Chem.* **294**, 2903–2912
38. Nandakumar, M., Prosser, G. A., de Carvalho, L. P. S., and Rhee, K. (2015) Metabolomics of *Mycobacterium tuberculosis*. In: Parish, T., Roberts, D. M., eds. *Mycobacteria Protocols*, Springer New York, New York, NY: 105–115
39. Maksymiuk, C., Balakrishnan, A., Bryk, R., Rhee, K. Y., and Nathan, C. F. (2015) E1 of alpha-ketoglutarate dehydrogenase defends *Mycobacterium tuberculosis* against glutamate anaplerosis and nitroxidative stress. *Proc. Natl. Acad. Sci. U. S. A.* **112**, E5834–5843
40. McNeil, M. B., Ryburn, H. W. K., Harold, L. K., Tirados, J. F., and Cook, G. M. (2020) Transcriptional inhibition of the F1F0-type ATP synthase has bactericidal consequences on the viability of mycobacteria. *Antimicrob. Agents Chemother.* **64**, e00492-20
41. Sambandamurthy, V. K., Wang, X., Chen, B., Russell, R. G., Derrick, S., Collins, F. M., Morris, S. L., and Jacobs, W. R., Jr. (2002) A pantothenate auxotroph of *Mycobacterium tuberculosis* is highly attenuated and protects mice against tuberculosis. *Nat. Med.* **8**, 1171–1174
42. Fedrizzi, T., Meehan, C. J., Grottola, A., Giacobazzi, E., Fregni Serpini, G., Tagliazucchi, S., Fabio, A., Bettua, C., Bertorelli, R., De Sanctis, V., Rumpianesi, F., Pecorari, M., Jousson, O., Tortoli, E., and Segata, N. (2017) Genomic characterization of nontuberculous mycobacteria. *Sci. Rep.* **7**, 45258
43. Altschul, S. F., Gish, W., Miller, W., Myers, E. W., and Lipman, D. J. (1990) Basic local alignment search tool. *J. Mol. Biol.* **215**, 403–410
44. UniProt Consortium (2019) UniProt: A worldwide hub of protein knowledge. *Nucleic Acids Res.* **47**, D506–D515
45. Asnicar, F., Weingart, G., Tickle, T. L., Huttenhower, C., and Segata, N. (2015) Compact graphical representation of phylogenetic data and metadata with GraPhlAn. *PeerJ* **3**, e1029